The International Journal of Advanced Manufacturing Technology (2019) 100:2971–2980
https://doi.org/10.1007/s00170-018-2891-z

ORIGINAL ARTICLE

Joining of elements fabricated by a robotized laser/wire directed energy deposition process by using an autogenous laser welding

Meysam Akbari[1] · Radovan Kovacevic[1]

Received: 7 August 2018 / Accepted: 12 October 2018 / Published online: 23 October 2018
© Springer-Verlag London Ltd., part of Springer Nature 2018

Abstract
A robotized laser/wire directed energy deposition (RLW-DED) process has been employed, specifically in applications where higher deposition rates or larger buildup envelopes are needed. However, this process might have limitations in printing certain complex shape parts. Fabricating parts with overhang sections, depending on the geometry, might cause a collision between the laser head and the buildup. Part segmentation and joining the elements back together has been presented to overcome those limitations. In this study, the welding of additively manufactured parts by RLW-DED has been proposed. Autogenous laser welding, performed at the same setup used for RLW-DED, was utilized to join the thin-walled 316LSi DED parts. Mechanical and microstructural testing were then performed on the welded samples. The results showed that the mechanical properties of welded DED parts are comparable with those of DED parts. Furthermore, a component of complex shape was fabricated to show the capability of the developed process. Therefore, the welding of RLW-DED parts can expand the application of 3D-printed parts in industry.

Keywords Laser wire directed energy deposition · Welding · Microstructure · Mechanical properties · Complex parts · Joining

1 Introduction

Robotized laser/wire directed energy deposition (RLW-DED) as a metal-based additive manufacturing (AM) technology has been gaining attention. According to ISO/ASTM 52900:2015 [1] and ASTM F3187-16 [2], DED is defined as "an additive manufacturing process in which focused thermal energy is used to fuse materials by melting as they are being deposited." DED is accomplished by feeding of metallic powder or wire into the melt pool formed by a highly focused energy source such as laser, electron beam, or arc. For instance, Williams et al. [3] employed wire and arc to produce large titanium parts (> 10 kg). They also evaluated the residual stress in the buildups. Abioye et al. [4] used laser as a heat source and Inconel wire to fabricate multi-layer coatings in order to increase the corrosion resistance of stainless steel components. They showed that the coating could well protect the parts exposed to corrosion. Brandl et al. [5] utilized laser and wire to manufacture multi-layer depositions. They characterized the microstructural properties of buildups and showed that grain dimensions at single beads can be used to qualitatively indicate microstructural and mechanical properties. Industry is noticing DED's capability to fabricate near-net-shape metal parts with higher deposition rates. Using a low-cost welding wire as feedstock and a robot as a kinematic system provides a high flexibility to print complex geometries with dimensional accuracy within ± 0.5 mm [6]. Also, some efforts have been made in RLW-DED process by means of vision system, to increase the process stability [7] and predict and control the mechanical and microstructural properties of the buildup in real time [8]. However, there exist some limitations in printing certain parts in the DED process. For instance, a part with very complex form or intrinsic features could be difficult to fabricate even with a robotized system. In the DED process, there is no support material. This lack of support is unlike the powder bed fusion (PBF) process, in which the melt pool is always supported by the metal powder in the bed. In DED, the motion system, mainly the po-

✉ Radovan Kovacevic
kovacevi@lyle.smu.edu

[1] Research Center for Advanced Manufacturing, Southern Methodist University, 3101, Dyre Street, Dallas, TX 75205, USA

sitioning table, provides the possibility for the melt pool to get support from the previously deposited layer. However, in special cases, for example, in fabricating a part with an overhang section, the positioning table needs to be tilted in a large angle to be able to build the overhang section. Many researchers developed different methods in the DED process for fabricating the overhang parts. Zhang et al. [9] developed an adaptive slicing algorithm to build non-uniform thickness layer due to the change in the build direction. By using this technique, they were able to build the overhang parts. Dwivedi et al. [10] developed an algorithm to fabricate branching slender structures. However, adding more overhang sections or branches to the existing overhang part makes the geometry and thereby the path planning very complex. Moreover, there might be possible inaccessibility of laser head to the part and eventually a collision could happen. Therefore, segmenting part into smaller sub-parts and joining the elements back together could be a solution to deal with those limitations in the DED process to some extent. For instance, a slender branched larger structure could be divided into several easy to print sub-parts and then joined back together. It should be noted that, in complex geometries, the part should be segmented at locations with no structurally-critical intersections.

Very few studies focused on joining of AM parts. Casalino et al. [11] studied the possibility of joining selective laser-melted (SLM) parts to wrought stainless steel parts by using fiber hybrid laser-arc welding. Then they evaluated the efficiency of the welding process. Wits et al. [12] achieved good quality welds by adjusting process parameters in a laser welding of SLM titanium parts. Also, Matilainen et al. [13] investigated the weldability of SLM 316L components to cold-rolled sheet metal 316L parts in terms of the existence of pores and cracks in the weld area. However, to the authors' knowledge, no study was found in the literature that focused on joining the DED parts by using an autogenous laser welding process.

Autogenous laser welding has been used extensively in joining applications where the higher welding speed and a lower heat input are desired. Different laser types such as fiber laser, disk laser, CO_2 laser, or diode laser could be used in such applications. This process can also provide a very small heat-affected zone (HAZ), low heat distortion, and narrow and deep penetration, and eventually can produce joints with a high quality [14]. It is also suitable for welding of dissimilar materials with high quality joints and small HAZ [15]. Laser could also offer a better absorptivity in welding a broad range of materials. In the present investigation, a robotized laser/wire directed energy deposition system followed by an autogenous fiber laser welding were utilized to boost the flexibility of the DED process. This process is considered as a hybrid system since it combines two processes to fabricate a part. This process broadened the range of DED applications. The main objective of this paper was to investigate the mechanical and microstructural properties of the butt welds between the DED thin-wall parts obtained by the autogenous laser welding.

2 Experimental procedure

2.1 Materials

The feedstock material used in this study was an austenitic stainless steel (316LSi) in the form of wire from ESAB with a diameter of 1.2 mm. Also, a commercially-available 304L stainless steel plate with a thickness of 6 mm was utilized as a support plate (substrate). The chemical compositions of wire and substrate are given in Table 1.

2.2 Methodology

A robotized laser/wire directed energy deposition system (RLW-DED) was used to fabricate the parts. Figure 1 illustrates the experimental setup. A 6-axis KUKA robot (KR-60) coupled with a 2-axis rotary table was used to provide the kinematics of the deposition system. A 4 kW fiber laser with 1070 nm wavelength from IPG was utilized as a heat source. A Precitec YW50 laser welding head was mounted on the robot arm to deliver the laser beam to the processing zone. The laser beam was defocused at 10 mm below the focal point, resulting in 1.6-mm beam spot diameter. Also, in order to feed the wire, a Binzel wire feeding system with two synchronized push and pull motors was used. Moreover, slicing the STL file of the 3D model and generating the toolpath and code for the robot controller were done in SKM DCAM offline programming software. The same setup without the wire feeder was used also for autogenous laser welding of the DED parts.

Four thin-walled coupons of the same geometry and dimensions were built by using a RLW-DED system as shown in Fig. 2a. All the beads in coupons were deposited

Table 1 Chemical compositions of wire and substrate

Element (wt%)	C	Mn	Si	Ni	Mo	Cr	Cu	P	S	Fe
Wire (316LSi)	0.01	1.8	0.9	12.2	2.60	18.4	0.12	0.03	0.03	Bal.
Substrate (304L)	0.03	2	–	8	–	18	–	0.045	0.03	Bal.

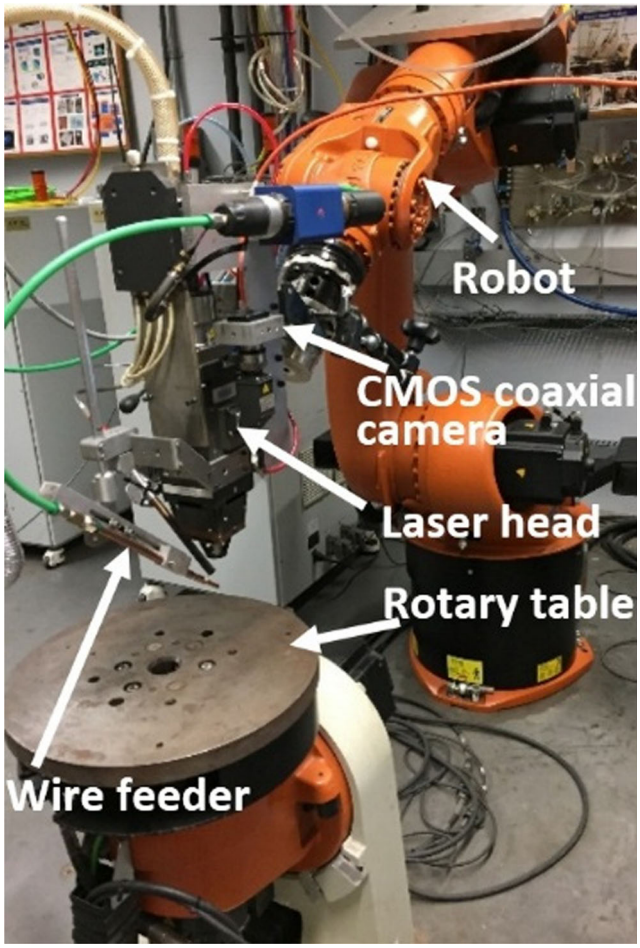

Fig. 1 A robotized laser/wire directed energy deposition system used for DED and welding processes

in one direction as shown in Fig. 2b, c. Three beads were deposited per layer to achieve 4 mm thickness of the wall. After each track was deposited, the laser head was positioned for the next bead. The idle time to position the laser head was kept at a low level by adjusting the robot speed at higher speed of 250 mm/s. The coupons were machined before the welding process in order to make the DED plates with a precise and consistent thickness for butt welding, and then welded together. Figure 2b, c shows the configurations of welds and orientation of tensile samples with respect to joints and DED parts. Two coupons were welded together such that the tensile samples were cut out "parallel" to the direction of the DED beads in the "deposition" direction as depicted in Fig. 2b. This configuration is called Weld DED-P for simplicity. Two other coupons were joined in such a way that the tensile samples were taken out "normal" to the deposition direction as indicated in Fig. 2c. This configuration is referred to as Weld DED-N in the rest of this paper. In the Weld DED-N specimens, the tensile loading direction was normal to the sliced layers. The reason for considering the tensile samples in two directions was to involve the effects of inherent anisotropic mechanical behavior of the DED parts. In each type of configuration, three tensile specimens were prepared. Figure 2d, e depict the welded DED parts. In addition, two sets of samples, one normal and the other parallel to the deposition direction, were prepared from DED parts without joints. Therefore, larger buildups were necessary to meet the size of the standard tensile specimen. Two thin-walled coupons with the same size, one for making normal tensile specimens and the other for making parallel ones, were fabricated as shown in Fig. 3a–c. The purpose of preparing tensile samples without a weld was to compare their tensile properties to those properties of the welded DED specimens. The tensile samples taken from the

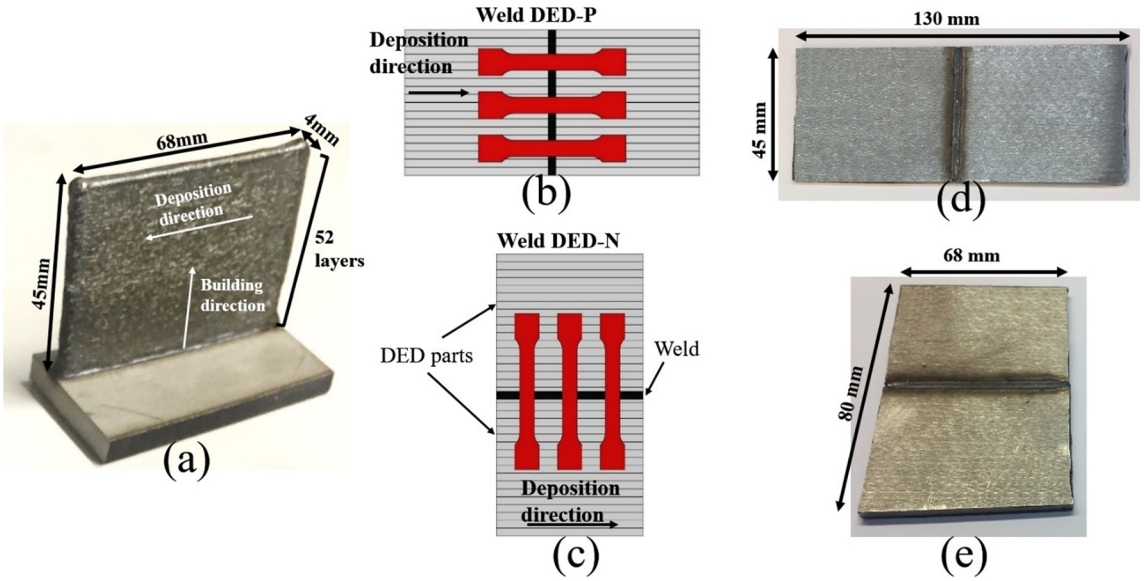

Fig. 2 **a** As-built coupon used for welding. **b** Weld DED-P sample: tensile specimens parallel to the deposition direction. **c** Weld DED-N sample: tensile specimens normal to the deposition direction (**d**, **e**) welded DED parts

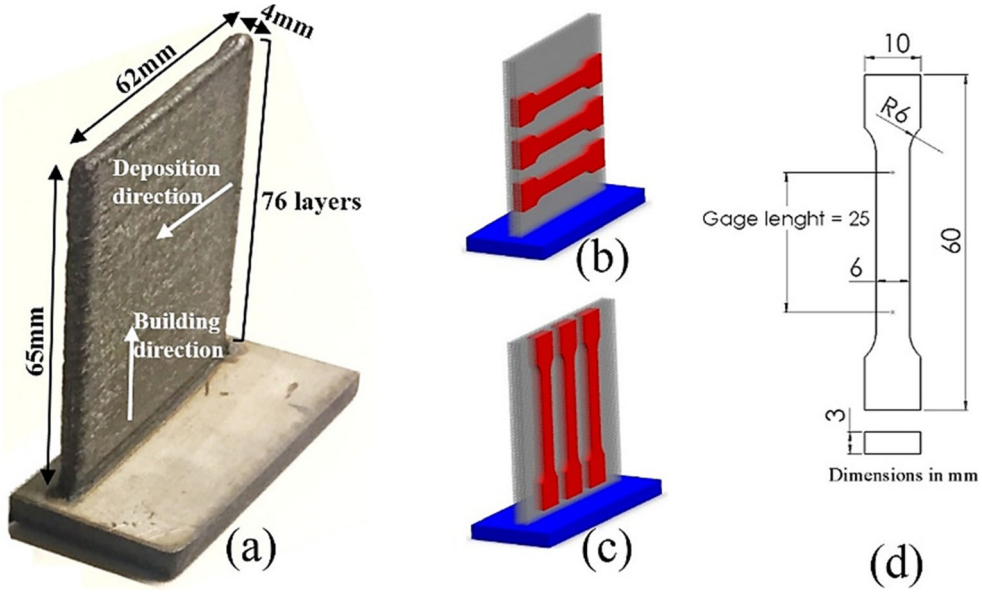

Fig. 3 **a** As-built coupon for preparing tensile specimens without weld. **b** Orientation of tensile specimens in the parallel direction (DED-P). **c** Orientation of tensile specimens in the normal direction (DED-N). **d** The dimensions of the standard tensile specimen per ASTM E8 [17]

DED part without a weld were designated as DED-P and DED-N specimens, that is, those specimens in the parallel and normal direction relative to the deposition direction, respectively. The processing parameters used for the RLW-DED process and autogenous laser welding are provided in Table 2. The main process variables such as laser power, travel speed, wire feed speed, Z-increment, and overlap increment were optimized in the previous work [6]. The optimized process parameters provided the constant and stable deposition on the entire build. The RLW-DED was conducted in an open atmosphere; therefore, in order to achieve a successful process, it is necessary to protect the melt pool. An inert gas (Argon) was used to shield the melt pool from oxidation. Shielding could also improve the properties of deposition and eventually promote the inter-layer bonding by providing better surface wetting [16]. A side-feeding nozzle with respect to the laser head was used to feed the Argon with the flow rate of 15 l/min and 30 l/min for DED and welding processes, respectively. The parameters for the welding process were optimized by welding several dummy samples of wrought plates with 3 mm thickness. The dimensions of the tensile specimens used in this study were selected according to the ASTM E08 standard [17] as shown in Fig. 3d. After welding, the tensile samples were cut out by using a waterjet cutting machine and were ground to remove the face and root of the welds.

Tensile tests were performed on an Instron 5582 tensile test machine with 1 mm/min strain rate at room temperature. In order to capture the elongation (strain) during the tensile test, the crosshead displacement of the machine was used. Also, to verify the value of elongation to failure of specimens obtained from the machine crosshead, all the specimens were marked before the test based on the gage length and after the test the broken parts were put back together to measure the elongation to failure. The cross-sections of the joints were mounted, sanded, and polished using a diamond polishing pad. Then, the samples were chemically etched in a solution of (HCL:HNO3 = 3:1) for 40 s. Microstructural analysis of the welds was conducted by using an optical microscope (Olympus DP72) and scanning electron microscopy (SEM LEO 1450) equipped with an energy dispersive spectroscopy (EDS). A Vickers microhardness tester machine (Clark-CM700) was utilized to perform microhardness measurements. A load of 1 kg with the waiting time of 15 s was applied during microhardness test. A fracture surface analysis was also done by the same SEM.

Table 2 Processing parameters for DED and welding

Process	Laser power (W)	Travel speed (mm/s)	Shielding gas flow rate (l/min)	Wire feed speed (mm/s)	Z-increment (mm)	Overlap increment (mm)
DED	1000	8	15 (Argon)	12	0.85	1.35
Welding*	2900	30	30 (Argon)	–	–	–

*The focal point was positioned at the top surface of the plates

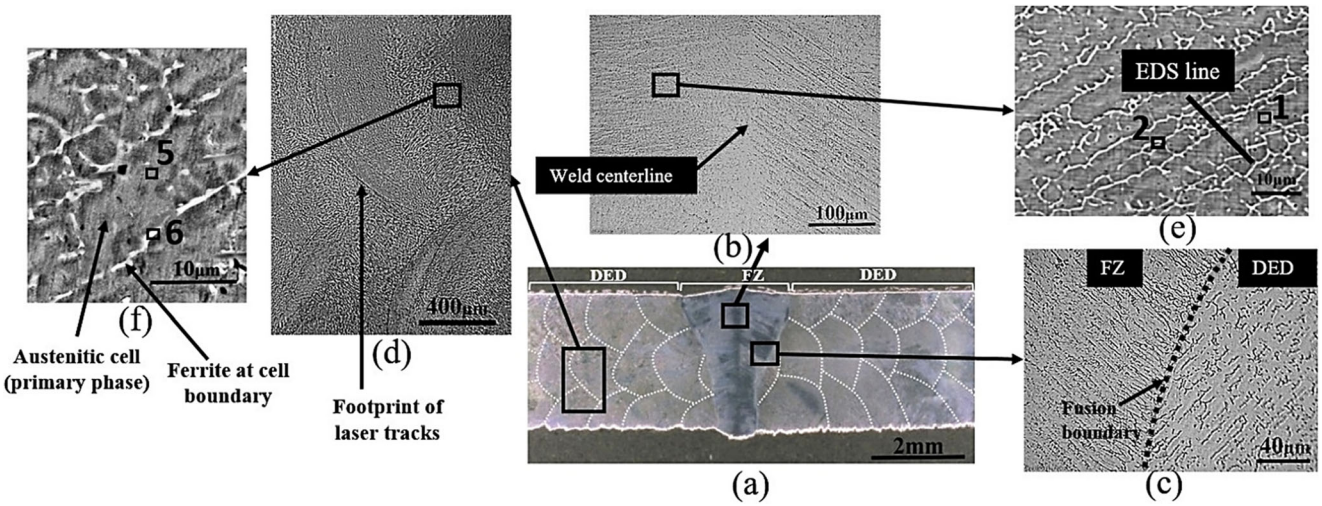

Fig. 4 The transverse-section images of Weld DED-N sample. **a** Optical micrograph showing the weld zone and DED plates. **b** Distribution of grains around weld centerline. **c** Fusion boundary. **d** DED microstructure. **e** SEM image of the weld zone indicating the columnar dendrites. **f** SEM image of the DED indicating the columnar dendrites

3 Experimental results and discussion

3.1 Microstructural analysis

Figures 4 and 5 show the cross-section microstructure of the Weld DED-N and Weld DED-P, respectively. In Figs. 4a and 5a, the footprint of laser tracks are indicated. The footprint of laser tracks are indicator of border of each new track that is being deposited in the cross sectional microstructure. This could be also recognized as melt pool boundary. Butt joints with full penetration were observed. The weld zone was found to be in a "Y" shape in both coupons with the widest dimension at the crown and the narrowest at the middle of the bead section as shown in Figs. 4a and 5a. Also, no HAZ was observed in the joints. This is attributed to the higher energy density and lower heat input of the laser welding process compared to arc-based welding methods such as GMAW. Due to the higher cooling rates in the laser welding process compared to GTAW, there is no sufficient time for grains that are located between fusion zone (FZ) and the base plates to grow, resulting in a joint without HAZ [18]. This is considered as a good characteristic of a laser-welded joint. No noticeable cracks or inclusions were found in the fusion zone. Due to the similar nature of laser welding and laser directed energy deposition during the process of solidification, the final morphology was found to be mainly columnar dendritic in both the weld zone and DED parts as shown in Fig. 4b, d. It can be seen from Fig. 4b that in the fusion zone, the dendrites were symmetrically distributed around the weld centerline. Also, dendrites were grown epitaxially from fusion boundary to the weld centerline, opposite to the heat flow direction [19]. In addition, the similar columnar dendritic structure directed from the bottom of the tracks toward the top was observed in the DED microstructure as shown in Fig. 4d. The magnified views of microstructure in the weld and DED are displayed in Fig. 4e, f and Fig. 5b. The dendritic structure is clear. The darker areas are the primary dendrite cells that were consisted of the austenite (γ) phase. The lighter area between dendrites was the skeletal δ-ferrite phase. During the solidification of the weld zones and DED of 316LSi, due to the high cooling rates associated

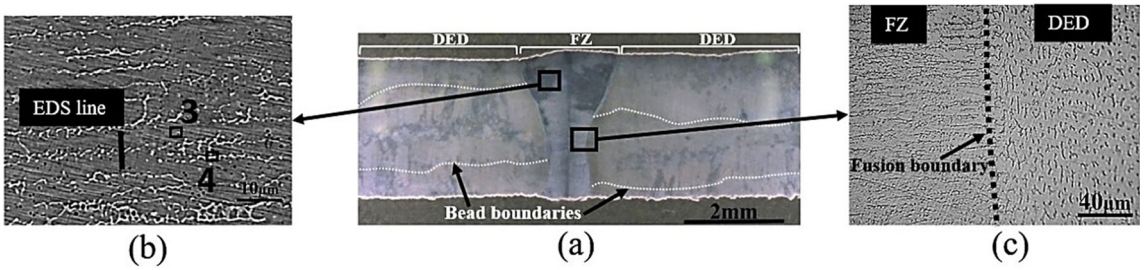

Fig. 5 The transverse-section optical images of Weld DED-P sample. **a** Optical micrograph showing the weld zone and DED plates. **b** SEM image of the weld zone indicating the columnar dendrites. **c** Fusion boundary

with laser material processing, the $\delta \rightarrow \gamma$ transformation remained incomplete. Thereby, formation of the skeletal δ-ferrite in the austenitic matrix was the result [20]. Therefore, the final solidification mode of the material either in the weld zone or DED was found to be ferritic-austenitic (FA). The primary dendrite arm spacing in the weld zone for both Weld DED-N and Weld DED-P coupons was about 2.5–5 μm; whereas, this value for the DED part was about 4–10 μm. The finer dendrite size in the weld zone clearly signified relatively higher cooling rate and lower heat input in the welding process compared to those experienced in the DED process. Figures 4c and 5c also demonstrate the fusion boundary between the DED parts and weld fusion zone. The transition in the size of grains from DED to weld was clear.

In order to study the variations in distribution of elements in the weld zone and DED parts, the EDS analysis was performed, and the results are shown in Fig. 6 and Table 3. Figures 6a, b show the EDS scanning line for Cr and Ni elements in the weld zone of the Weld DED-N and Weld DED-P samples, respectively. The lines are shown in Fig. 4e and Fig. 5b. No noticeable segregation can be seen from the EDS profiles that could increase the degree of homogeneity, mechanical properties, and the pitting corrosion resistance of the austenitic stainless steel welds [21, 22]. Also, the alloying elements distribution in different points located on the dendritic austenite matrix and δ-ferrite were measured as depicted in Table 3. In this Table, the weight content of alloying elements in DED was compared to those in the weld zone. The weight content of chrome, as expected, was slightly lower at all points in the austenitic phase both in the weld area and the DED parts. However, the Ni weight content was slightly higher in these areas. These results revealed no significant segregation. Thereby a uniform chemical composition was presented throughout the entire fusion zone and the DED parts.

Table 3 EDS chemical composition of different points across the weld zone and DED parts

	Weld				DED	
Element	Point 1 Wt%	Point 2 Wt%	Point 3 Wt%	Point 4 Wt%	Point 5 Wt%	Point 6 Wt%
Si	0.92	0.66	0.69	0.71	0.81	0.87
Mo	2.92	2.79	3.29	3.02	2.12	2.45
Cr	18.85	19.22	18.78	19.71	19.77	20.66
Fe	63.87	66.65	64.9	66.9	64.55	65.66
Ni	13.44	10.69	12.34	10.66	12.26	10.51

3.2 Tensile properties

Tensile testing with the standard specimen taken from the welded DED parts and DED parts (Figs. 2 and 3) were conducted to evaluate the ultimate tensile strength (UTS) and elongation to failure of the samples. The typical stress-strain curves of all specimens are illustrated in Fig. 7a. The typical broken tensile specimens are also shown in this Figure. All tensile specimens of the welded coupons were fractured in DED parts, demonstrating that the good quality welds were achieved. The average values of UTS and elongation along with their relevant error bar that indicate the range for each value are presented in Fig. 7b. It can be seen from Fig. 7b that the UTS and elongation of specimens from the Weld DED-P and DED-P coupons were higher than those from the Weld DED-N and DED-N coupons. In other words, regardless of whether the tensile specimen had a joint or not, the specimen showed higher tensile properties if it was aligned parallel to the direction of deposition. These results indicated the anisotropic mechanical behavior of the DED parts. The lower UTS and ductility of specimens in the normal direction might be attributed to weaker metallurgical bonding, presence of imperfections such as inter-layers/beads pores caused by lack-of-fusion in DED

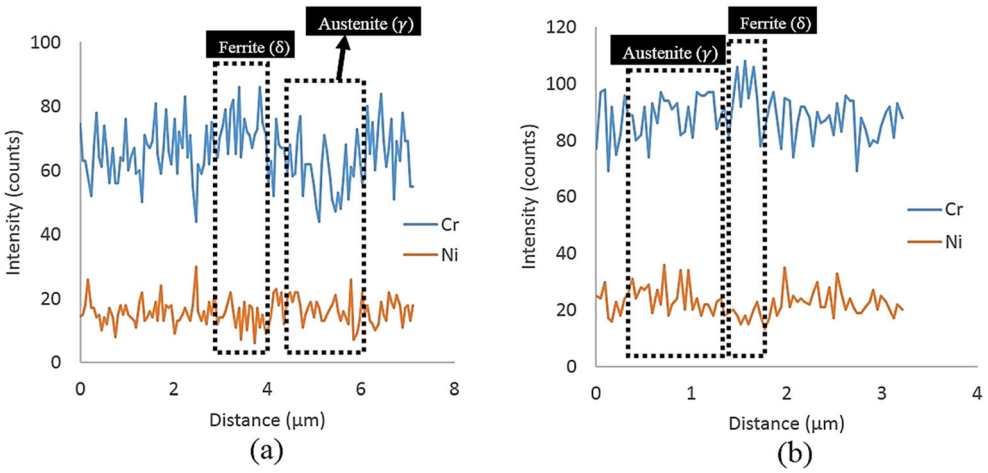

Fig. 6 EDS line profiles of Cr and Ni elements across the phase boundaries for **a** Weld DED-N and **b** Weld DED-P coupons. The scanning lines are shown in Figs. 4e and 5b

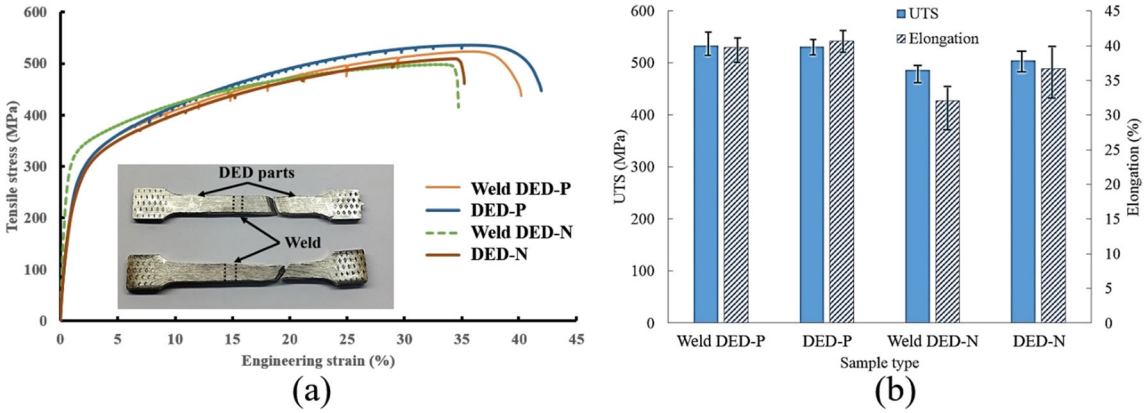

Fig. 7 Tensile test results for DED and welded DED specimens. **a** Typical stress-strain curves of different specimens along with broken tensile specimens. **b** The average UTS and elongation values of all tested specimens

parts, epitaxial grain growth during solidification, and orientation of dentrites in the microstructure. The lack-of-fusion is the major source of porosity in the as-deposited parts that are usually caused by insufficient melting, mostly occurred at the layer interface [23]. Furthermore, by comparing the Weld DED-P to DED-P specimens or Weld DED-N to DED-P specimens, it can be deduced that the existence of weld joints did not have a negative effect on the tensile properties of the DED parts. In the commonly-used laser welding of wrought plates, the joints usually indicated better mechanical properties compared to the wrought base plate. This result is because the microstructure of welds changed greatly [24, 25]. However, in the laser welded DED parts, the mechanical properties were not improved after welding, since the microstructure and chemical composition of the joints remained very similar to those of DED (e.g., columnar dendritic microstructure).

Figure 8a, b show the SEM fracture surfaces of the Weld DED-N and Weld DED-P coupons, respectively. The orientation of fracture surface was about 45° to the specimen axis that is evidence of ductile fracture (see also Fig. 7a). At the higher magnifications (Fig. 8c, d), fine and uniform dimples were predominantly observed, indicating the failure of samples in a ductile manner. Moreover, some torn belts in the fracture surface associated with columnar dendritic structure were observed.

3.3 Microhardness

Vickers microhardness measurements were performed across the fusion zone as depicted in Fig. 9. No significant difference between microhardness of the fusion zone and DED parts was observed. The average microhardness values for the fusion

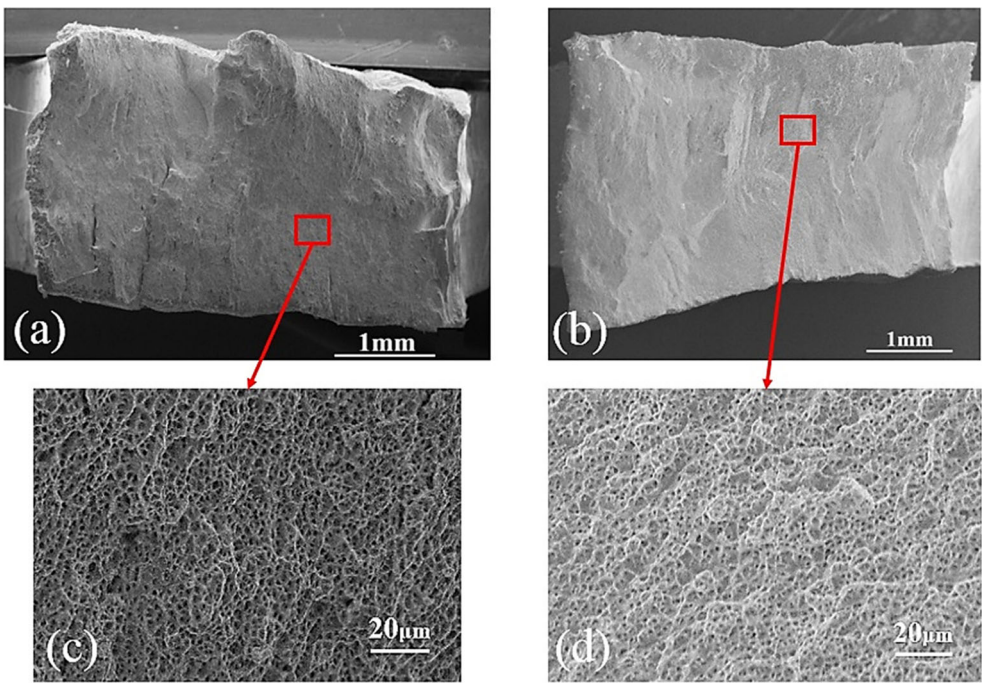

Fig. 8 Typical tensile fracture surfaces. **a** Weld DED-N specimen. **b** Weld DED-P specimen (**c**, **d**) dimples in the fracture surfaces showing the ductile fracture

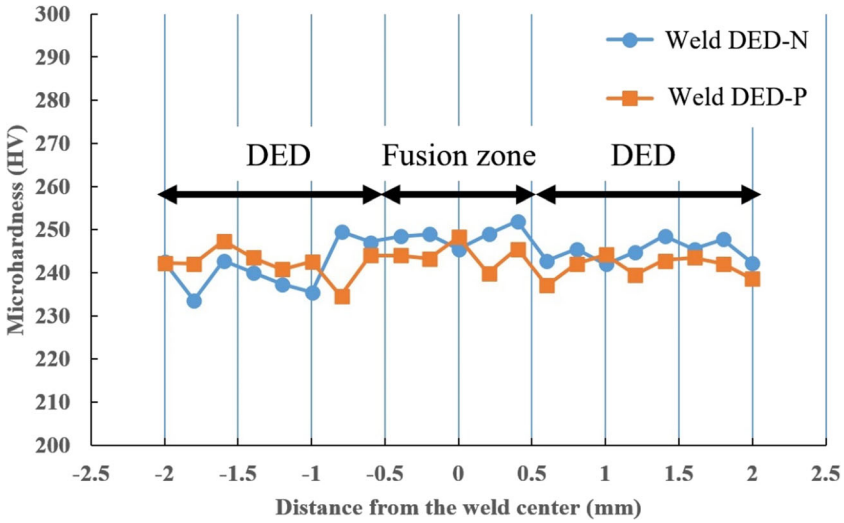

Fig. 9 Microhardness profiles along the cross-sections of the joints

zone and DED parts were about 247 HV and 242 HV, respectively. The hardness is a result of grain size, meaning that finer microstructure results in higher microhardness [26]. The grain boundaries act as barrier for dislocations and eventually smaller grain size would have higher microhardness [26]. Owing to the identical grain morphology, as discussed earlier, and close values of grain size between the DED and weld zone, a uniform hardness profile across the DED and fusion zone was obtained.

3.4 Porosity

Figure 10a, b illustrate the SEM micrographs of the transverse cross-sections of Weld DED-N and Weld DED-P samples, respectively. A few macropores were observed in both DED and fusion zone. Generally, the main source of pores in the welding process is due to the gas entrapment during the solidification process and is found mostly in spherical shape [27, 28]. The pores in the weld zone of DED parts might have two sources of formation. They may either come from the already existing pores in the DED parts that were generated mainly due to the lack-of-fusion or they might be formed in the welding process as a result of gas entrapment. The DED process is prone to the production of microscopic or even macroscopic voids. Upon welding the DED parts, some of the pores may escape from the fusion zone and some of them may combine to form larger pores. The porosity was found to be scattered in the weld zone, similar to the distribution of pores in DED parts. The size of the porosity was found to be within the range of approximately 18–35 μm in both DED and fusion zone.

4 A case of fabricating a part with overhang surface

To further verify the capability of the developed process, a part with an overhang section was selected. One of the challenges in the DED process is building complex parts with overhang sections. As an example, a part that was composed of two cones is illustrated in Fig. 11a. It should be noted that the part is a thin-walled structure, where the thickness of wall was equal to the width of a bead. Therefore, a spiral path planning was selected to avoid multiple start-finishes of the process. Building the lower cone is feasible by titling the rotary table for angle α (Fig. 11b). During the deposition of the lower

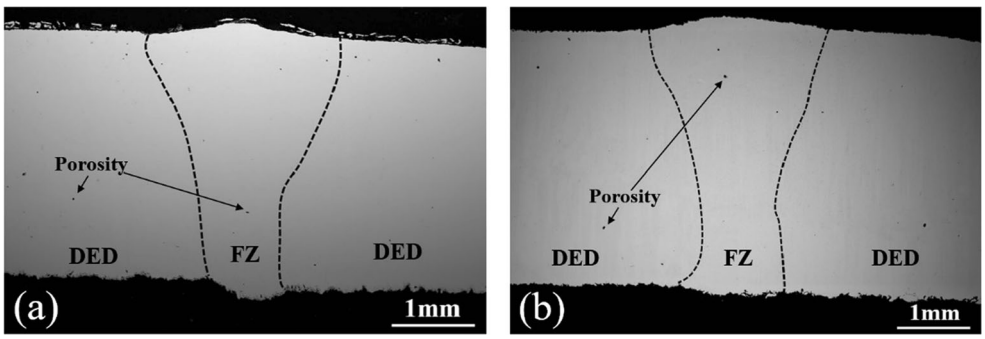

Fig. 10 Porosity obsereved in **a** Weld DED-N and **b** Weld DED-P coupons

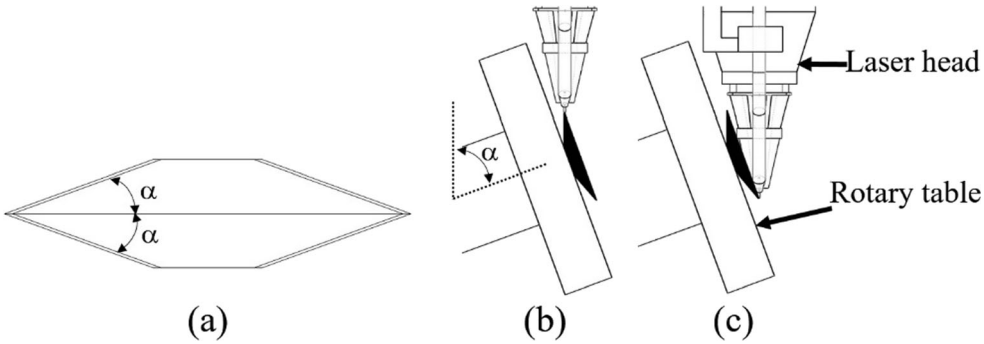

Fig. 11 **a** A part with overhang sections. **b** Illustration of kinematic system when the lower cone was printed. **c** The occurrence of collision between laser head and lower cone at the instance when the upper cone started to be printed

cone, the tilting angle of the rotary table was fixed. Then, after the lower cone was printed, the process should be stopped for repositioning the laser head. The process started deposition of the upper cone on the last layer of the lower cone (Fig. 11c). Figure 11b shows the instance when the lower cone is being printed. Figure 11c illustrates an instance when the printing of the upper cone is begun.

However, under the higher values of the angle (α), there might be a collision between the laser head and lower cone as can be seen from Fig. 11c. Thus, it would be impossible to continue printing of the upper overhang section. Moreover, in the position that is shown in Fig. 11c, the melt pool was partially supported by the lower cone, leading to instability in the process. Therefore, for such a case, printing the cones individually and then joining them in order to fabricate the whole part could be a solution. Figure 12a, b show the lower and upper cones that were printed by the RLW-DED process. Then, an autogenous laser welding process was used to join the cones together on the rotary table (Fig. 12c). The same process parameters given in Table 2 were used to fabricate the slopped component. This part was fabricated to show the application of laser welding in joining the DED parts. The angle (α) in this case was 35°; however, this part could be fabricated with higher angles.

Fig. 12d also demonstrates the cross-section of the weld. A good joint was achieved, confirming the capability of autogenous laser welding in joining thin-walled DED parts. The results proved that the flexibility of the DED process in printing certain complex geometries, especially overhang structures, could be improved.

5 Conclusions

In this investigation, an autogenous laser welding process was applied to join the thin-walled elements fabricated by a robotized laser/wire directed energy deposition system. This hybrid system showed the capability of fabricating complex geometries that are difficult to build by using DED process. Microstructural analysis revealed sound welds with almost no HAZ. The dominant grain morphology either in the weld zone or DED parts was found to be columnar dendritic, since autogenous laser welding and laser directed energy deposition processes have identical solidification behavior. The alloying elements distribution showed a uniform chemical composition in the weld and DED parts with minimum segregation. Also, the mechanical test results showed no significant difference between the welded DED parts and DED parts without weld,

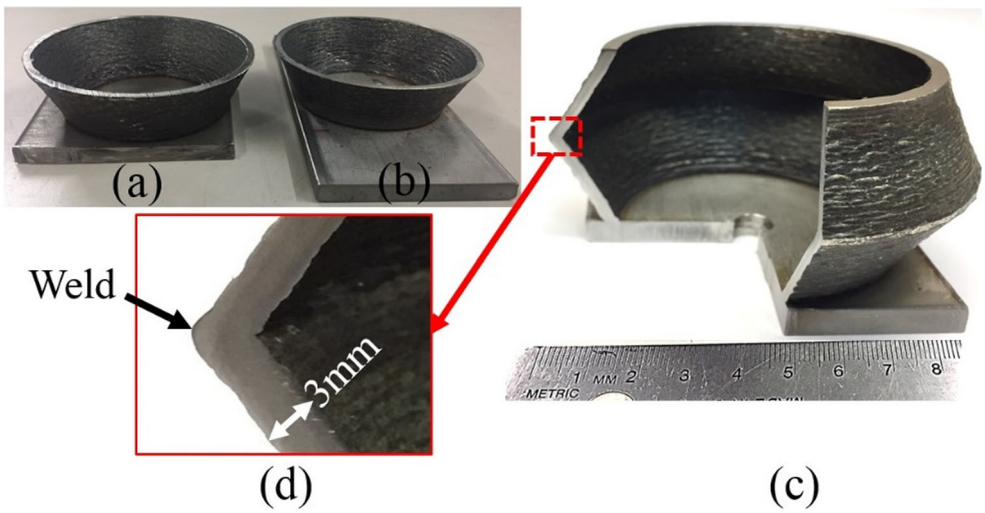

Fig. 12 **a**, **b** The lower and upper cones fabricated by RLW-DED. **c** The final part after autogenous laser welding of two cones. **d** The cross-section of the joint

in terms of UTS and elongation to failure. However, the tensile specimens taken from normal direction relative to the deposition direction indicated lower UTS and elongation, revealing the anisotropic mechanical behavior of DED parts. Microhardness distribution results showed no noticeable difference between the fusion zone and DED parts, owing to the close size of the grains in these two areas.

Eventually, this study demonstrated that some limitations in DED process such as fabricating parts with overhang sections could be solved by part segmentation and then joining the elements back together by an autogenous laser welding. Therefore, product design in DED process could obtain more flexibility.

Acknowledgements The authors would like to thank Andrew Socha, the research engineer at Research Center for Advanced Manufacturing, for his assistance during experimental works.

Funding information This study was supported by NSF's Grant No. IIP-1539853.

Publisher's Note Springer Nature remains neutral with regard to jurisdictional claims in published maps and institutional affiliations.

References

1. Additive Manufacturing—General Principles—Terminology (2015) ISO/ASTM 52900. International Organization for Standardization, Geneva
2. ASTM F3187–16, standard guide for directed energy deposition of metals, ASTM International, West Conshohocken, PA, 2016, www.astm.org
3. Williams SW, Martina F, Addison AC, Ding J, Pardal G, Colegrove P (2016) Wire+ arc additive manufacturing. Mater Sci Technol 32(7):641–647
4. Abioye TE, McCartney DG, Clare AT (2015) Laser cladding of Inconel 625 wire for corrosion protection. J Mater Process Technol 217:232–240
5. Brandl E, Michailov V, Viehweger B, Leyens C (2011) Deposition of Ti–6Al–4V using laser and wire, part I: microstructural properties of single beads. Surf Coat Technol 206(6):1120–1129
6. Akbari M, Ding Y, Kovacevic R. Process development for a robotized laser wire additive manufacturing. In ASME 2017 12th International Manufacturing Science and Engineering Conference collocated with the JSME/ASME 2017 6th International Conference on Materials and Processing 2017 Jun 4 (pp. V002T01A015-V002T01A015). American Society of Mechanical Engineers
7. Heralić A, Christiansson AK, Ottosson M, Lennartson B (2010) Increased stability in laser metal wire deposition through feedback from optical measurements. Opt Lasers Eng 48(4):478–485
8. Akbari M, Kovacevic R (2018) An investigation on mechanical and microstructural properties of 316LSi parts fabricated by a robotized laser/wire direct metal deposition system. Addit Manuf 23:487–497
9. Zhang J, Liou F (2004) Adaptive slicing for a multi-axis laser aided manufacturing process. J Mech Des 126(2):254–261
10. R. Dwivedi R, S. Zekovic, R. Kovacevic. A novel approach to fabricate uni-directional and branching slender structures using laser-based direct metal deposition. Int J Mach Tools Manuf 2007;47(7–8):1246–1256
11. Casalino G, Campanelli SL, Ludovico AD (2013) Laser-arc hybrid welding of wrought to selective laser molten stainless steel. Int J Adv Manuf Technol 68(1–4):209–216
12. Wits WW, Becker JJ (2015) Laser beam welding of titanium additive manufactured parts. Procedia CIRP 28:70–75
13. Matilainen VP, Pekkarinen J, Salminen A (2016) Weldability of additive manufactured stainless steel. Phys Procedia 83:808–817
14. Salminen A, Westin E, Lappalainen E, Unt A (2012) Effect of gas shielding and heat input on autogenous welding of duplex stainless steel. ICALEO2012
15. Berretta JR, de Rossi W, das Neves MD, de Almeida IA, Junior ND (2007) Pulsed Nd:YAG laser welding of AISI 304 to AISI 420 stainless steels. Opt Lasers Eng 45(9):960–966
16. Oshida Y (2010) Bioscience and bioengineering of titanium materials. Elsevier
17. Standard AS. E8," standard test methods for tension testing of metallic materials. Annual book of ASTM standards 2004;3:57–72
18. Yan J, Gao M, Zeng X (2010) Study on microstructure and mechanical properties of 304 stainless steel joints by TIG, laser and laser-TIG hybrid welding. Opt Lasers Eng 48(4):512–517
19. Cui CY, Cui XG, Ren XD, Liu TT, Hu JD, Wang YM (2013) Microstructure and microhardness of fiber laser butt welded joint of stainless steel plates. Mater Des 49:761–765
20. Silva CC, de Miranda HC, de Sant'Ana HB, Farias JP (2009) Microstructure, hardness and petroleum corrosion evaluation of 316L/AWS E309MoL-16 weld metal. Mater Charact 60(4):346–352
21. Kwok CT, Fong SL, Cheng FT, Man HC (2006) Pitting and galvanic corrosion behavior of laser-welded stainless steels. J Mater Process Technol 176(1–3):168–178
22. Vilpas M (1999) Prediction of microsegregation and pitting corrosion resistance of austenitic stainless steel welds by modelling. Technical Research Centre of Finland
23. Kobryn PA, Moore EH, Semiatin SL (2000) The effect of laser power and traverse speed on microstructure, porosity, and build height in laser-deposited Ti-6Al-4V. Scr Mater 43(4):299–305
24. Zambon A, Ferro P, Bonollo F (2006) Microstructural, compositional and residual stress evaluation of CO2 laser welded superaustenitic AISI 904L stainless steel. Mater Sci Eng A 424(1–2):117–127
25. Cao X, Jahazi M (2009) Effect of welding speed on butt joint quality of Ti–6Al–4V alloy welded using a high-power Nd: YAG laser. Opt Lasers Eng 47(11):1231–1241
26. Gao M, Zeng X, Yan J, Hu Q (2008) Microstructure characteristics of laser–MIG hybrid welded mild steel. Appl Surf Sci 254(18):5715–5721
27. Seto N, Katayama S, Matsunawa A (2000) High-speed simultaneous observation of plasma and keyhole behavior during high power CO 2 laser welding: effect of shielding gas on porosity formation. J Laser Appl 12(6):245–250
28. Katayama S, Kobayashi Y, Mizutani M, Matsunawa A (2001) Effect of vacuum on penetration and defects in laser welding. J Laser Appl 13(5):187–192